Acta Mech. Sin. (2016) 32(1):38–53
DOI 10.1007/s10409-015-0526-2

RESEARCH PAPER

Effect of quadratic pressure gradient term on a one-dimensional moving boundary problem based on modified Darcy's law

Wenchao Liu[1,2] · **Jun Yao**[2] · **Zhangxin Chen**[3] · **Yuewu Liu**[1]

Received: 30 May 2015 / Revised: 27 July 2015 / Accepted: 20 September 2015 / Published online: 29 October 2015

Abstract A relatively high formation pressure gradient can exist in seepage flow in low-permeable porous media with a threshold pressure gradient, and a significant error may then be caused in the model computation by neglecting the quadratic pressure gradient term in the governing equations. Based on these concerns, in consideration of the quadratic pressure gradient term, a basic moving boundary model is constructed for a one-dimensional seepage flow problem with a threshold pressure gradient. Owing to a strong nonlinearity and the existing moving boundary in the mathematical model, a corresponding numerical solution method is presented. First, a spatial coordinate transformation method is adopted in order to transform the system of partial differential equations with moving boundary conditions into a closed system with fixed boundary conditions; then the solution can be stably numerically obtained by a fully implicit finite-difference method. The validity of the numerical method is verified by a published exact analytical solution. Furthermore, to compare with Darcy's flow problem, the exact analytical solution for the case of Darcy's flow considering the quadratic pressure gradient term is also derived by an inverse Laplace transform. A comparison of these model solutions leads to the conclusion that such moving boundary problems must incorporate the quadratic pressure gradient term in their governing equations; the sensitive effects of the quadratic pressure gradient term tend to diminish, with the dimensionless threshold pressure gradient increasing for the one-dimensional problem.

Keywords Quadratic pressure gradient term · Threshold pressure gradient · Porous media · Numerical solution · Moving boundary

1 Introduction

Owing to high international oil and gas prices and decreasing production output from conventional reservoirs, such unconventional petroleum resources as low-permeability oil and gas reservoirs, shale gas, and heavy-oil reservoirs have attracted increasing attention in the petroleum industry in recent years. Concomitantly, the relevant research on the nonlinear kinematic principles for the seepage flow behavior in these unconventional reservoirs (porous media) is very intense [1–27] at present. It has been demonstrated from abundant physical experiments and theories [1,8,9,14–16,18–20,23–25,28–39] that the seepage flow in low-permeability porous media and the seepage flow of Bingham non-Newtonian fluids do not obey the classical Darcy's law [40] (Fig. 1): a threshold pressure gradient exists. In particular, using the fractal approach, Cai [41] investigated the problem of seepage flow of non-Newtonian fluids in low-permeability porous media and obtained the threshold pressure gradient. This means that fluid flow happens only if the formation pressure gradient is larger than the threshold pressure gradient.

Further research on these relevant moving boundary models has been conducted [7,8,10–12,21,22,30,42–46]. The

✉ Wenchao Liu
wcliu_2008@126.com

[1] Institute of Mechanics, Chinese Academy of Sciences, Beijing 100190, China

[2] School of Petroleum Engineering, China University of Petroleum (Huadong), Qingdao 266580, China

[3] Department of Chemical and Petroleum Engineering, Schulich School of Engineering, University of Calgary, Calgary, AB T2N 1N4, Canada

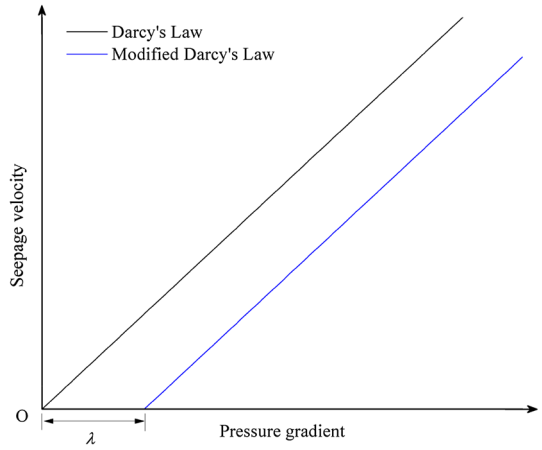

Fig. 1 Kinematic equations of Darcy's law and modified Darcy's law

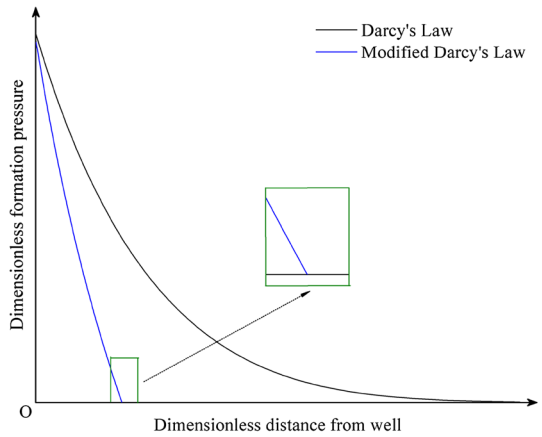

Fig. 2 Difference in computed dimensionless formation pressure distribution curves

computed formation pressure distributions for these moving boundary problems of seepage flow with a threshold pressure gradient (modified Darcy's law [29]) are unlike those for earlier Darcy's flow models (Fig. 2): The formation pressure decreases with larger slope, i.e., higher formation pressure gradient as the distance increases, and the curve can exhibit compact support [2]; however, the formation pressure distribution curve of Darcy's flow is much more smooth. The relatively higher formation pressure gradient of seepage flow with a threshold pressure gradient can be attributed to the physical reason that the threshold pressure gradient slows down the propagation of a pressure drop, and then causes a high pressure gradient in small pressure-disturbed regions.

In the modeling of seepage flow, the dependence of rock porosity and fluid density on formation pressure in forms of exponential functions can lead to nonlinear effects [47]. The deduced governing equation always contains a nonlinear quadratic pressure gradient term. The general computation of this governing equation usually neglects the nonlinear quadratic pressure gradient term [48]. For most routine engineering applications in the development of conventional reservoirs, the error in implementing this linearization may be acceptable. However, the linearization by neglecting the quadratic pressure gradient term is not applicable for large values of time [49,50]; furthermore, the proposition of small formation pressure gradients may cause significant errors in predicting the formation pressure, in particular for certain operations (or situations) [51] such as, for example, hydraulic fracturing, high wellbore injection or production rates, well testing, large pressure pulse testing, and wellbore skin effect. For conventional Darcy's flow models, using a Laplace transform, Odeh and Badu [52] presented analytical solutions to nonlinear partial differential equations (PDEs) taking into consideration the quadratic pressure gradient term, describing the seepage flow of a slightly compressible fluid; it was concluded that the nonlinear solutions showed the pressure difference for injection and pumping conditions, in comparison with the generally accepted solutions of linearized equations. Finjord et al. [53] obtained constant-rate analytical solutions of a one-phase radial flow equation, considering the effect of the quadratic pressure gradient term, in an oil reservoir with constant diffusivity and compressibility. Wang and Dusseault [54] developed an analytical solution for pore pressure coupled with deformation in porous media; the quadratic pressure gradient term was taken into account, and it was shown that existing solutions deviated when the pressure gradient was high. Chakrabarty et al. [51,55] conducted research on analytical solutions of nonlinear radial flow systems using a Laplace transform and concluded that serious errors could be caused by neglecting the quadratic pressure gradient term in some cases, such as high injection rates in flow systems with small transmissivity; it was also demonstrated that the standard condition allowing the quadratic gradient term to be neglected was incorrect. Braeuning et al. [56] studied a problem of the effect of quadratic pressure gradient term on variable-rate well tests; it was concluded that wellbore damage, pseudo-skin, and a nonlinear flow parameter could affect the error caused by the linearization. Cao et al. [49] obtained the exact analytical solutions of nonlinear seepage flow models, including quadratic pressure gradient terms for the two cases of constant production rate and constant wellbore pressure, using the generalized Weber transform and Hankel transform; their resulting analysis showed that the effect of the quadratic pressure gradient term in long-term well tests should be considered. Marshall [47] studied nonlinear models of compressible fluid flow through porous media, taking into consideration both the quadratic pressure gradient term and the pressure-dependent hydraulic diffusivity, using the Cole–Hopf transformation for linearization, and following a Laplace transformation; his research results indicated that compressibility effects could be neglected at

ambient temperature, but in some geothermal systems with higher pressure and temperature the underlying state equation of the fluid was applicable. Li et al. [57] constructed a mathematical flow model in a fractal multilayer reservoir in consideration of both the quadratic pressure gradient term and wellbore storage and presented its analytical solution in a Laplace domain; their analysis showed that the solution involved similar structures. Dewei et al. [58] analytically investigated a nonlinear mathematical model of transient seepage flow incorporating the quadratic pressure gradient term; it was found that a comprehensive unsteady flow model with a wellbore skin effect should retain the quadratic pressure gradient term. Bai et al. [48] incorporated the quadratic pressure gradient term in the space of a fracture and built a dual porosity model; its solution was analytically obtained by a Hankel transform; their study indicated that for cases of high rate of wellbore injection and production and significant compressibility of fractures, it was suitable to simulate naturally fractured reservoirs using the constructed model. Tong et al. [50] presented some exact analytical solutions of a nonlinear dual-porosity model taking into consideration the quadratic pressure gradient term by the Hankel and Weber transforms; they concluded that long-term well testing should consider the effect of the quadratic pressure gradient term. Nie et al. [59] presented a nonlinear flow model with a quadratic pressure gradient term for a dual-porosity reservoir and obtained a solution through a variable substitution for linearization; it was found that the effect of the quadratic pressure gradient term was large, especially for unconventional reservoirs. Yao et al. [60] established a mathematical model of seepage flow in a double-porosity and fractal reservoir, solved using a Laplace transform; their study indicated that neglecting the quadratic pressure gradient term could lead to 10 % relative errors in the modeling of dual-porosity and fractal reservoirs. Nie et al. [61] studied a nonlinear well testing model in a triple-porosity reservoir with fractures and vugs, and a quadratic pressure gradient term was considered; the analytical solution of the model was obtained using a Laplace transform, and it was also demonstrated, through numerical tests and an example of well testing interpretation, that the type curves of a nonlinear model deviated obviously from those of a linear model and the values obtained from a nonlinear model explanation were more accurate.

As far as we know, for moving boundary problems of seepage flow with a threshold pressure gradient, the effect of a quadratic pressure gradient term has rarely been taken into account in the governing equations [7,8,10–12,21,22,30,42–46]. However, neglecting this nonlinear quadratic pressure gradient term may generate large errors in the relevant modeling and computation; after all, the formation pressure gradient for seepage flow with a threshold pressure gradient is higher. Furthermore, in modern times, the development of advanced analysis methods and improved resolutions of pressure measurement machines [51] makes it necessary to quantitatively study the effect of the quadratic pressure gradient term. It is important to mention that simultaneously considering other particular situations (e.g., high wellbore injection or production rates, wellbore skin effect) as discussed in the literature may lead to an even bigger effect of the quadratic pressure gradient term. And to clearly figure out the effect of the quadratic pressure gradient term for the basic seepage flow problem in low-permeability porous media based on the principle of modified Darcy's flow [29], those aspects are not incorporated into the moving boundary model; research on the effect of their interplay will be undertaken sometime in the future.

Hence, based on these concerns, the quadratic pressure gradient term is simply incorporated into the modeling of a basic moving boundary problem of one-dimensional seepage flow with a threshold pressure gradient. Owing to the strong nonlinearity of the moving boundary model, it cannot be solved analytically. Here, a spatial coordinate transform method [8,62–64] is adopted first to equivalently transform the moving boundary problem into a closed nonlinear PDE system with fixed boundary conditions; then it can be solved numerically using a stable, fully implicit finite-difference method. The validity of the numerical method is verified by a published exact analytical solution [10]. Then, using the numerical results, the effect of this quadratic pressure gradient term can be discussed and analyzed quantitatively with respect to different values of dimensionless threshold pressure gradients. Moreover, the effects of the quadratic pressure gradient term on the solutions of these models based on the modified Darcy's law (the threshold pressure gradient is not equal to zero) can also be compared to its effects on solutions [10] based on Darcy's law.

2 Mathematical modeling

A one-dimensional seepage flow problem with a threshold pressure gradient is investigated here; the porous medium is assumed to be semi-infinitely long, homogeneous, isotropic, isothermal, and slightly compressible; a production well has a constant production rate at the inner boundary; the effect of gravity is neglected; and the fluid is slightly compressible.

The state equation of the fluid density is [47,54,61]:

$$\rho = \rho_0 \exp\left[-C_{\mathrm{f}}\left(p_0 - p\right)\right], \tag{1}$$

where ρ is the fluid density, ρ_0 is the initial fluid density, p_0 is the initial pressure, p is the pressure, and C_{f} is the compressibility coefficient of the fluid.

The state equation of a rock is as follows [47,54,61]

$$\phi = \phi_0 \exp\left[-C_\phi \left(p_0 - p\right)\right], \tag{2}$$

where ϕ is the porosity of the porous medium, ϕ_0 is the initial porosity, and C_ϕ is the compressibility coefficient of the porosity.

The modified Darcy's law for seepage flow with a threshold pressure gradient is as follows [29]

$$\upsilon = \begin{cases} 0, & 0 \leqslant \frac{\mathrm{d}p}{\mathrm{d}x} \leqslant \lambda, \\ -\frac{k}{\mu} \cdot \left(\frac{\mathrm{d}p}{\mathrm{d}x} - \lambda\right), & \frac{\mathrm{d}p}{\mathrm{d}x} > \lambda, \end{cases} \tag{3}$$

where k is the permeability of the porous medium, μ the fluid viscosity, x the distance, υ the seepage velocity, and λ the threshold pressure gradient.

The continuity equation for the one-dimensional seepage flow is as follows [8,10,43]

$$-\frac{\partial}{\partial x}\left(\rho\upsilon\right) = \frac{\partial\left(\rho\phi\right)}{\partial t}, \quad 0 \leqslant x \leqslant s\left(t\right), \tag{4}$$

where t is time and s is the moving boundary.

The governing equation, considering the nonlinear quadratic pressure gradient term, can be deduced by substituting Eqs. (1)–(3) into Eq. (4), as follows (Appendix 1)

$$\frac{\partial^2 p}{\partial x^2} + C_\mathrm{f} \cdot \left(\frac{\partial p}{\partial x}\right)^2 = \frac{\mu\phi_0 C_\mathrm{t}}{k} \cdot \frac{\partial p}{\partial t}, \tag{5}$$

where C_t is the total compressibility coefficient.

The initial conditions are as follows

$$s\left(0\right) = 0, \tag{6}$$

$$p|_{t=0} = p_0. \tag{7}$$

The inner boundary condition is

$$\left.\frac{k}{\mu}\left(\frac{\partial p}{\partial x} - \lambda\right)\right|_{x=0} = \upsilon_\mathrm{w}, \quad \lambda > 0, \tag{8}$$

where υ_w is the constant flow rate.

The moving boundary conditions are

$$p|_{x=s(t)} = p_0, \tag{9}$$

$$\left.\frac{\partial p}{\partial x}\right|_{x=s(t)} = \lambda. \tag{10}$$

Equations (5)–(10) together form a mathematical model of one-dimensional seepage flow with a threshold pressure gradient, taking into consideration the quadratic pressure gradient term.

The dimensionless parameters are written as follows

$$x_\mathrm{D} = \frac{x}{x_\mathrm{w}}, \tag{11}$$

$$t_\mathrm{D} = \frac{k}{\mu\phi_0 C_\mathrm{t} x_\mathrm{w}^2} t, \tag{12}$$

$$\delta = \frac{s}{x_\mathrm{w}}, \tag{13}$$

$$P_\mathrm{D} = \frac{k}{\upsilon_\mathrm{w} x_\mathrm{w} \mu}\left(p_0 - p\right), \tag{14}$$

$$\lambda_\mathrm{D} = \frac{k\lambda}{\upsilon_\mathrm{w}\mu}, \tag{15}$$

$$\alpha_\mathrm{D} = \frac{\upsilon_\mathrm{w}\mu x_\mathrm{w}, C_\mathrm{f}}{k}, \tag{16}$$

where x_w is the constant distance for nondimensionalization, x_D is the dimensionless distance, t_D is the dimensionless time, P_D is the dimensionless pressure, α_D is the dimensionless compressibility, λ_D is the dimensionless threshold pressure gradient, and δ is the dimensionless moving boundary.

The following Eqs. (17)–(22) constitute a dimensionless mathematical model that takes into consideration the quadratic threshold pressure gradient:

$$\frac{\partial^2 P_\mathrm{D}}{\partial x_\mathrm{D}^2} - \alpha_\mathrm{D}\left(\frac{\partial P_\mathrm{D}}{\partial x_\mathrm{D}}\right)^2 = \frac{\partial P_\mathrm{D}}{\partial t_\mathrm{D}}, \quad 0 \leqslant x_\mathrm{D} \leqslant \delta\left(t_\mathrm{D}\right), \tag{17}$$

$$P_\mathrm{D}|_{t_\mathrm{D}=0} = 0, \tag{18}$$

$$\delta\left(0\right) = 0, \tag{19}$$

$$\left.\frac{\partial P_\mathrm{D}}{\partial x_\mathrm{D}}\right|_{x_\mathrm{D}=0} = -\left(1 + \lambda_\mathrm{D}\right), \tag{20}$$

$$\left.\frac{\partial P_\mathrm{D}}{\partial x_\mathrm{D}}\right|_{x_\mathrm{D}=\delta(t_\mathrm{D})} = -\lambda_\mathrm{D}, \tag{21}$$

$$P_\mathrm{D}|_{x_\mathrm{D}=\delta(t_\mathrm{D})} = 0. \tag{22}$$

The coefficient of the dimensionless quadratic pressure gradient term, i.e., the dimensionless compressibility α_D, can be used to analyze the effect of the quadratic pressure gradient term on the moving boundary problem. In fact, from its definition, i.e., Eq. (16), the physical description of the dimensionless compressibility α_D can be provided. First, Eq. (16) can be rewritten equivalently by combining some physical variables according to the specific physical meaning as $\alpha_\mathrm{D} = (\upsilon_\mathrm{W} x_\mathrm{W})/(k/\mu)C_\mathrm{f}$. If x_w is assumed to be the width of the one-dimensional flow for certain flow cases, $\upsilon_\mathrm{W} \cdot x_\mathrm{W}$ can represent the whole flow rate, and k/μ represents the mobility. Then it can be seen that the dimensionless compressibility α_D relates to three factors—the whole flow rate, the mobility, and the compressibility of the fluid—and the value of the dimensionless compressibility α_D is proportional

to the whole flow rate and the compressibility coefficient of the fluid, but inversely proportional to the mobility.

From Eq. (22) we have

$$P_{\mathrm{D}}\left(\delta\left(t_{\mathrm{D}}\right), t_{\mathrm{D}}\right)=0. \tag{23}$$

Differentiating the two sides of Eq. (23) with respect to t_{D}, we have

$$\left.\frac{\partial P_{\mathrm{D}}}{\partial t_{\mathrm{D}}}\right|_{x_{\mathrm{D}}=\delta\left(t_{\mathrm{D}}\right)}+\left.\frac{\partial P_{\mathrm{D}}}{\partial x_{\mathrm{D}}}\right|_{x_{\mathrm{D}}=\delta\left(t_{\mathrm{D}}\right)} \cdot \frac{\partial \delta}{\partial t_{\mathrm{D}}}=0. \tag{24}$$

Substituting Eq. (21) into Eq. (24) yields

$$\left.\frac{\partial P_{\mathrm{D}}}{\partial t_{\mathrm{D}}}\right|_{x_{\mathrm{D}}=\delta\left(t_{\mathrm{D}}\right)}=\lambda_{\mathrm{D}} \cdot \frac{\partial \delta}{\partial t_{\mathrm{D}}}. \tag{25}$$

Let $x_{\mathrm{D}}=\delta\left(t_{\mathrm{D}}\right)$ on both sides of Eq. (17), and then substituting Eq. (21) yields

$$\left.\frac{\partial P_{\mathrm{D}}}{\partial t_{\mathrm{D}}}\right|_{x_{\mathrm{D}}=\delta\left(t_{\mathrm{D}}\right)}=\left.\frac{\partial^2 P_{\mathrm{D}}}{\partial x_{\mathrm{D}}^2}\right|_{x_{\mathrm{D}}=\delta\left(t_{\mathrm{D}}\right)}-\alpha_{\mathrm{D}} \cdot \lambda_{\mathrm{D}}^2. \tag{26}$$

The velocity of the moving boundary can be deduced through Eqs. (25) and (26) as follows

$$\frac{\partial \delta}{\partial t_{\mathrm{D}}}=\frac{1}{\lambda_{\mathrm{D}}}\left.\frac{\partial^2 P_{\mathrm{D}}}{\partial x_{\mathrm{D}}^2}\right|_{x_{\mathrm{D}}=\delta\left(t_{\mathrm{D}}\right)}-\alpha_{\mathrm{D}} \cdot \lambda_{\mathrm{D}}. \tag{27}$$

Equation (27) indicates that considering the quadratic pressure gradient term can reduce the velocity of a moving boundary when α_{D} is not equal to zero.

3 Numerical solution method

In the mathematical model, the seepage flow region contains a moving boundary with time increasing [8]. Obviously, it is hardly possible to implement spatial discretization directly during a numerical solution process. To solve this problem, a spatial coordinate transformation method is introduced as follows [8,62–64]

$$y_{\mathrm{D}}\left(x_{\mathrm{D}}, t_{\mathrm{D}}\right)=\frac{x_{\mathrm{D}}}{\delta\left(t_{\mathrm{D}}\right)}. \tag{28}$$

Through Eq. (28), the dynamic flow region with moving boundary $[0, \delta(t_{\mathrm{D}})]$ can be transformed into a fixed region [0, 1]; correspondingly, the differential variables can be transformed, respectively, as follows

$$\frac{\partial P_{\mathrm{D}}}{\partial x_{\mathrm{D}}}=\frac{\partial P_{\mathrm{D}}}{\partial y_{\mathrm{D}}} \cdot \frac{1}{\delta}, \tag{29}$$

$$\frac{\partial^2 P_{\mathrm{D}}}{\partial x_{\mathrm{D}}^2}=\frac{\partial^2 P_{\mathrm{D}}}{\partial y_{\mathrm{D}}^2} \cdot \frac{1}{\delta^2}, \tag{30}$$

$$\frac{\partial P_{\mathrm{D}}}{\partial t_{\mathrm{D}}}=\frac{\partial P_{\mathrm{D}}}{\partial t_{\mathrm{D}}}-\frac{\partial P_{\mathrm{D}}}{\partial y_{\mathrm{D}}} \cdot \frac{\partial \delta}{\partial t_{\mathrm{D}}} \cdot \frac{y_{\mathrm{D}}}{\delta}. \tag{31}$$

Using Eqs. (29)–(31), Eq. (17) can be transformed as follows

$$\frac{\partial^2 P_{\mathrm{D}}}{\partial y_{\mathrm{D}}^2} \cdot \frac{1}{\delta^2}-\alpha_{\mathrm{D}}\left(\frac{\partial P_{\mathrm{D}}}{\partial y_{\mathrm{D}}} \cdot \frac{1}{\delta}\right)^2=\frac{\partial P_{\mathrm{D}}}{\partial t_{\mathrm{D}}}-\frac{\partial P_{\mathrm{D}}}{\partial y_{\mathrm{D}}} \cdot \frac{\partial \delta}{\partial t_{\mathrm{D}}} \cdot \frac{y_{\mathrm{D}}}{\delta}, \quad 0 \leqslant y_{\mathrm{D}} \leqslant 1. \tag{32}$$

Using Eqs. (29)–(31), Eqs. (20)–(22) and Eq. (27) can be transformed, respectively, as follows

$$\left.\frac{\partial P_{\mathrm{D}}}{\partial y_{\mathrm{D}}} \cdot \frac{1}{\delta}\right|_{y_{\mathrm{D}}=0}=-\left(1+\lambda_{\mathrm{D}}\right), \tag{33}$$

$$\left.\frac{\partial P_{\mathrm{D}}}{\partial y_{\mathrm{D}}} \cdot \frac{1}{\delta}\right|_{y_{\mathrm{D}}=1}=-\lambda_{\mathrm{D}}, \tag{34}$$

$$P_{\mathrm{D}}|_{y_{\mathrm{D}}=1}=0, \tag{35}$$

$$\frac{\partial \delta}{\partial t_{\mathrm{D}}}=\frac{1}{\lambda_{\mathrm{D}}} \cdot \left.\frac{\partial^2 P_{\mathrm{D}}}{\partial y_{\mathrm{D}}^2}\right|_{y_{\mathrm{D}}=1} \cdot \frac{1}{\delta^2}-\alpha_{\mathrm{D}} \cdot \lambda_{\mathrm{D}}. \tag{36}$$

Substituting Eq. (36) into Eq. (32) yields

$$\begin{aligned}&\frac{\partial^2 P_{\mathrm{D}}}{\partial y_{\mathrm{D}}^2} \cdot \delta-\alpha_{\mathrm{D}} \cdot \delta \cdot\left(\frac{\partial P_{\mathrm{D}}}{\partial y_{\mathrm{D}}}\right)^2 \\ &=\frac{\partial P_{\mathrm{D}}}{\partial t_{\mathrm{D}}} \delta^3-\frac{\partial P_{\mathrm{D}}}{\partial y_{\mathrm{D}}} \cdot \frac{y_{\mathrm{D}}}{\lambda_{\mathrm{D}}} \cdot \left.\frac{\partial^2 P_{\mathrm{D}}}{\partial y_{\mathrm{D}}^2}\right|_{y_{\mathrm{D}}=1} \\ &\quad+\frac{\partial P_{\mathrm{D}}}{\partial y_{\mathrm{D}}} \cdot \alpha_{\mathrm{D}} \cdot \lambda_{\mathrm{D}} \cdot y_{\mathrm{D}} \cdot \delta^2.\end{aligned} \tag{37}$$

From Eq. (33) we have

$$\delta=-\left.\frac{\partial P_{\mathrm{D}}}{\partial y_{\mathrm{D}}}\right|_{y_{\mathrm{D}}=0} \cdot \frac{1}{1+\lambda_{\mathrm{D}}}. \tag{38}$$

Substituting Eq. (38) into Eq. (37) to cancel the variable δ yields

$$\begin{aligned}&\frac{\partial^2 P_{\mathrm{D}}}{\partial y_{\mathrm{D}}^2} \cdot \left.\frac{\partial P_{\mathrm{D}}}{\partial y_{\mathrm{D}}}\right|_{y_{\mathrm{D}}=0}-\alpha_{\mathrm{D}} \cdot\left(\frac{\partial P_{\mathrm{D}}}{\partial y_{\mathrm{D}}}\right)^2 \cdot \left.\frac{\partial P_{\mathrm{D}}}{\partial y_{\mathrm{D}}}\right|_{y_{\mathrm{D}}=0} \\ &-\frac{\partial P_{\mathrm{D}}}{\partial t_{\mathrm{D}}} \cdot\left(\left.\frac{\partial P_{\mathrm{D}}}{\partial y_{\mathrm{D}}}\right|_{y_{\mathrm{D}}=0}\right)^3 \cdot \frac{1}{\left(1+\lambda_{\mathrm{D}}\right)^2}-\frac{\partial P_{\mathrm{D}}}{\partial y_{\mathrm{D}}} \cdot \frac{\left(1+\lambda_{\mathrm{D}}\right)}{\lambda_{\mathrm{D}}} \\ &\cdot y_{\mathrm{D}} \cdot \left.\frac{\partial^2 P_{\mathrm{D}}}{\partial y_{\mathrm{D}}^2}\right|_{y_{\mathrm{D}}=1} \\ &+\frac{\partial P_{\mathrm{D}}}{\partial y_{\mathrm{D}}} \cdot \alpha_{\mathrm{D}} \cdot \lambda_{\mathrm{D}} \cdot y_{\mathrm{D}} \cdot\left(\left.\frac{\partial P_{\mathrm{D}}}{\partial y_{\mathrm{D}}}\right|_{y_{\mathrm{D}}=0}\right)^2 \cdot \frac{1}{1+\lambda_{\mathrm{D}}}=0.\end{aligned} \tag{39}$$

From Eq. (28), Eq. (18) can be transformed as

$$P_{\mathrm{D}}\left(y_{\mathrm{D}}, t_{\mathrm{D}}\right)|_{t_{\mathrm{D}}=0}=0. \tag{40}$$

From Eqs. (33) and (34) we have

$$\left.\frac{\partial P_{\mathrm{D}}}{\partial y_{\mathrm{D}}}\right|_{y_{\mathrm{D}}=0}=\frac{1+\lambda_{\mathrm{D}}}{\lambda_{\mathrm{D}}}\left.\frac{\partial P_{\mathrm{D}}}{\partial y_{\mathrm{D}}}\right|_{y_{\mathrm{D}}=1}. \tag{41}$$

A closed system of PDEs is formed through Eqs. (39)–(41) and Eq. (35). The transformed nonlinear system with respect to $P_{\mathrm{D}}(y_{\mathrm{D}}, t_{\mathrm{D}})$ is equivalent to the original model, but it has fixed boundary conditions. Here, its solution is stably numerically solved by a fully implicit finite-difference method [8,65]: the first derivative is replaced by a first-order forward difference, and the second derivative is replaced by a second-order central difference; then the difference equation of Eq. (39) is as follows

$$\begin{aligned}
&\frac{P_{\mathrm{D}i+1}^{j+1}-2P_{\mathrm{D}i}^{j+1}+P_{\mathrm{D}i-1}^{j+1}}{(\Delta y_{\mathrm{D}})^2}\cdot\frac{P_{\mathrm{D}1}^{j+1}-P_{\mathrm{D}0}^{j+1}}{\Delta y_{\mathrm{D}}}\\
&-\alpha_{\mathrm{D}}\cdot\left(\frac{P_{\mathrm{D}i+1}^{j+1}-P_{\mathrm{D}i}^{j+1}}{\Delta y_{\mathrm{D}}}\right)^2\cdot\frac{P_{\mathrm{D}1}^{j+1}-P_{\mathrm{D}0}^{j+1}}{\Delta y_{\mathrm{D}}}\\
&-\frac{P_{\mathrm{D}i}^{j+1}-P_{\mathrm{D}i}^{j}}{\Delta t_{\mathrm{D}}}\cdot\left(\frac{P_{\mathrm{D}1}^{j+1}-P_{\mathrm{D}0}^{j+1}}{\Delta y_{\mathrm{D}}}\right)^3\cdot\frac{1}{(1+\lambda_{\mathrm{D}})^2}\\
&-\frac{1+\lambda_{\mathrm{D}}}{\lambda_{\mathrm{D}}}\cdot i\cdot\Delta y_{\mathrm{D}}\cdot\frac{P_{\mathrm{D}i+1}^{j+1}-P_{\mathrm{D}i}^{j+1}}{\Delta y_{\mathrm{D}}}\cdot\frac{P_{\mathrm{D}N-2}^{j+1}-2P_{\mathrm{D}N-1}^{j+1}}{(\Delta y_{\mathrm{D}})^2}\\
&+\frac{P_{\mathrm{D}i+1}^{j+1}-P_{\mathrm{D}i}^{j+1}}{\Delta y_{\mathrm{D}}}\cdot\alpha_{\mathrm{D}}\cdot\lambda_{\mathrm{D}}\cdot i\cdot\Delta y_{\mathrm{D}}\cdot\left(\frac{P_{\mathrm{D}1}^{j+1}-P_{\mathrm{D}0}^{j+1}}{\Delta y_{\mathrm{D}}}\right)^2\\
&\cdot\frac{1}{1+\lambda_{\mathrm{D}}}=0,\quad i=1,2,\ldots,N-2,
\end{aligned} \tag{42}$$

where N denotes the total number of spatial grid subintervals with the same length; Δy_{D} is the length of a grid subinterval, which is equal to $1/N$; i denotes the index of the spatial grid from the well; j denotes the index of a time step; and Δt_{D} denotes the time step size.

From Eq. (35) we have

$$P_{\mathrm{D}N}^{j+1}=0. \tag{43}$$

Then, from Eqs. (42) and (43), when the index of the spatial grid is $(N-1)$, the difference equation can be written as follows

$$\begin{aligned}
&\frac{-2P_{\mathrm{D}(N-1)}^{j+1}+P_{\mathrm{D}(N-2)}^{j+1}}{(\Delta y_{\mathrm{D}})^2}\cdot\frac{P_{\mathrm{D}1}^{j+1}-P_{\mathrm{D}0}^{j+1}}{\Delta y_{\mathrm{D}}}\\
&-\alpha_{\mathrm{D}}\cdot\left(\frac{P_{\mathrm{D}(N-1)}^{j+1}}{\Delta y_{\mathrm{D}}}\right)^2\cdot\frac{P_{\mathrm{D}1}^{j+1}-P_{\mathrm{D}0}^{j+1}}{\Delta y_{\mathrm{D}}}\\
&-\frac{1}{(1+\lambda_{\mathrm{D}})^2}\left(\frac{P_{\mathrm{D}1}^{j+1}-P_{\mathrm{D}0}^{j+1}}{\Delta y_{\mathrm{D}}}\right)^3\cdot\frac{P_{\mathrm{D}(N-1)}^{j+1}-P_{\mathrm{D}(N-1)}^{j}}{\Delta t_{\mathrm{D}}}\\
&+\frac{1+\lambda_{\mathrm{D}}}{\lambda_{\mathrm{D}}}\cdot(N-1)\cdot\Delta y_{\mathrm{D}}\cdot\frac{P_{\mathrm{D}(N-1)}^{j+1}}{\Delta y_{\mathrm{D}}}\cdot\frac{P_{\mathrm{D}(N-2)}^{j+1}-2P_{\mathrm{D}(N-1)}^{j+1}}{(\Delta y_{\mathrm{D}})^2}\\
&-\frac{P_{\mathrm{D}(N-1)}^{j+1}}{\Delta y_{\mathrm{D}}}\cdot\alpha_{\mathrm{D}}\cdot\lambda_{\mathrm{D}}\cdot(N-1)\\
&\cdot\Delta y_{\mathrm{D}}\cdot\left(\frac{P_{\mathrm{D}1}^{j+1}-P_{\mathrm{D}0}^{j+1}}{\Delta y_{\mathrm{D}}}\right)^2\cdot\frac{1}{1+\lambda_{\mathrm{D}}}=0.
\end{aligned} \tag{44}$$

The difference equation of Eq. (41) is as follows

$$\frac{P_{\mathrm{D}1}^{j+1}-P_{\mathrm{D}0}^{j+1}}{\Delta y_{\mathrm{D}}}=-\frac{1+\lambda_{\mathrm{D}}}{\lambda_{\mathrm{D}}}\frac{P_{\mathrm{D}(N-1)}^{j+1}}{\Delta y_{\mathrm{D}}}. \tag{45}$$

From Eq. (40), the initial conditions are obtained as follows

$$P_{\mathrm{D}i}^{0}=0, i=0,1,2,\ldots,N-1. \tag{46}$$

Equations (42), (44), and (45) together form a group of nonlinear difference equations, which contains N equations and N unknown variables $P_{\mathrm{D}i}^{j+1}$ $(i=0,1,2,\ldots,N-1)$. The Newton–Raphson iterative method [8,65] is used to numerically solve these nonlinear difference equations. When the numerical solutions of $P_{\mathrm{D}i}^{j+1}$ $(i=0,1,2,\ldots,N-1)$ are obtained, j is replaced by $j+1$, and in the same manner the numerical solutions of N unknown variables $P_{\mathrm{D}i}^{j+2}$ $(i=0,1,2,\ldots,N-1)$ can also be obtained by the iterative method [8]; the rest can be deduced by analogy. Eventually, numerical solutions for the transformed system with respect to $P_{\mathrm{D}}(y_{\mathrm{D}}, t_{\mathrm{D}})$ can be obtained.

The difference equation of Eq. (28) is

$$x_{\mathrm{D}i}^{j+1}=y_{\mathrm{D}i}\cdot\delta^{j+1}. \tag{47}$$

The difference equation of Eq. (38) is

$$\delta^{j+1}=-\frac{P_{\mathrm{D}1}^{j+1}-P_{\mathrm{D}0}^{j+1}}{\Delta y_{\mathrm{D}}}\cdot\frac{1}{1+\lambda_{\mathrm{D}}}. \tag{48}$$

Substituting Eq. (48) into Eq. (47) yields

$$x_{\mathrm{D}i}^{j+1}=-i\cdot\frac{P_{\mathrm{D}1}^{j+1}-P_{\mathrm{D}0}^{j+1}}{1+\lambda_{\mathrm{D}}}. \tag{49}$$

By Eq. (49), numerical solutions of $P_{\mathrm{D}}(y_{\mathrm{D}}, t_{\mathrm{D}})$ can be transformed as those of $P_{\mathrm{D}}(x_{\mathrm{D}}, t_{\mathrm{D}})$ for every time step [8]. In fact, Eq. (49) indicates the time-dependent space discretization in the original spatial coordinate of x_{D}. However, in the transformed spatial coordinate of y_{D}, the space discretization is time-independent, which makes the finite difference solution more applicable and simpler [8].

4 Verification of numerical solution method

When the dimensionless compressibility is set to zero, the numerical solution of the moving boundary problem by the numerical method presented earlier can be compared with the already published exact analytical solution of this problem as follows [8,10]

$$P_{\mathrm{D}}(x_{\mathrm{D}}, t_{\mathrm{D}}) = 2(1+\lambda_{\mathrm{D}})\left[\theta\left(\frac{t_{\mathrm{D}}^{\frac{1}{2}} e^{-\frac{x_{\mathrm{D}}^2}{4t_{\mathrm{D}}}} + \frac{x_{\mathrm{D}}}{2}\pi^{\frac{1}{2}}\mathrm{erf}\left(\frac{x_{\mathrm{D}}}{2\sqrt{t_{\mathrm{D}}}}\right)}{e^{-\theta^2} + \pi^{\frac{1}{2}}\theta\mathrm{erf}(\theta)}\right) - \frac{x_{\mathrm{D}}}{2}\right], \quad x_{\mathrm{D}} \in [0, \delta], \tag{50}$$

where θ can be determined by the following equation [10]:

$$\frac{e^{-\theta^2}}{e^{-\theta^2} + \pi^{\frac{1}{2}}\theta\mathrm{erf}(\theta)} = \frac{\lambda_{\mathrm{D}}}{1+\lambda_{\mathrm{D}}}. \tag{51}$$

The equation for the distance of the moving boundary is as follows [8,10]

$$\delta = 2 \cdot \theta \cdot \sqrt{t_{\mathrm{D}}}. \tag{52}$$

Prada and Civan [29] conducted experiments on seepage flow in two types of low-permeability porous media (Brown sandstone #3 and Sandpack #3) with a threshold pressure gradient and obtained the actual experimental data. The dimensionless threshold pressure gradient can be evaluated from these data. The experimental data and the specific calculation process [8] are presented in Table 1. From Table 1, the two corresponding values of the dimensionless threshold pressure gradient λ_{D} can be calculated as 0.852 and 0.364, respectively. From Eq. (51), the values of θ can be computed as 0.6599 and 0.8889, respectively. Then from Eq. (50), the exact analytical solutions can be obtained.

For the numerical solution, we set $N = 160$, $\Delta t_{\mathrm{D}} = 10$, and $\alpha_{\mathrm{D}} = 0$. Figures 3, 4, and 5 show comparison curves between the numerical solutions and exact analytical solutions. These curves are plotted with respect to the dimensionless formation pressure distribution when $t_{\mathrm{D}} = 10000$, the dimensionless transient wellbore pressure and the dimensionless transient distance of the moving boundary, respectively. From Figs. 3, 4, and 5, it can be observed that the numerical solutions and the exact analytical solutions have good agreement [10]. Thus the correctness of our presented numerical method can be verified. Besides, from a large number of numerical experiments, it is known that as the length of the spatial grid decreases, the accuracy can be further improved [8], and the fully implicit finite-difference schemes can lead to unconditionally stable

Table 1 Calculation of dimensionless threshold pressure gradient λ_{D} with two groups of experimental data from Prada and Civan's flow experiments

Sample	λ (psi/cm)	k/μ (md/cp)	Minimum flow rate q_1 (cc/min)	Maximum flow rate q_2 (cc/min)	Cross-sectioanal area A (cm^2)	Average flow velocity $v_{\mathrm{w}} = (q_1+q_2)/A/2$ (cm/min)	$\lambda_D = \lambda k/\mu/v_{\mathrm{w}}$
Brown sandstone #3	0.0203	4730	1.71	17.5	20.2	0.475495	0.852
Sandpack #3	0.00548	23800	4.57	29.92	11.4	1.512719	0.364

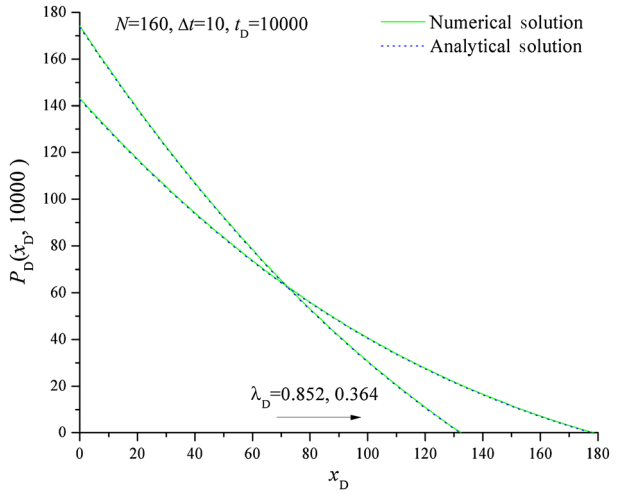

Fig. 3 Comparison of dimensionless formation pressure distribution under different values of dimensionless threshold pressure gradient

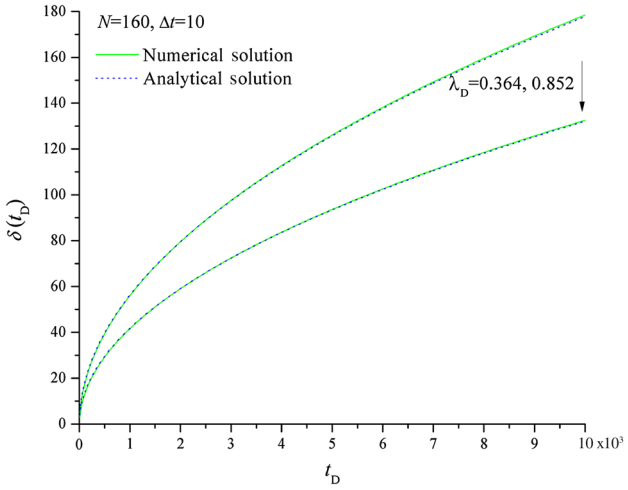

Fig. 5 Comparison of dimensionless transient distance of moving boundary under different values of dimensionless threshold pressure gradient

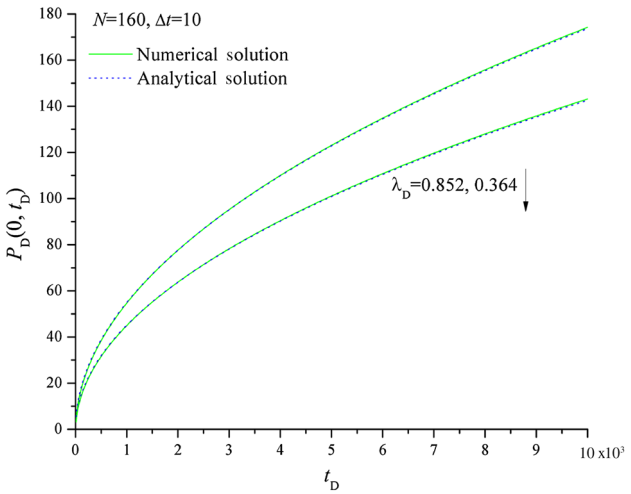

Fig. 4 Comparison of dimensionless transient wellbore pressure under different values of dimensionless threshold pressure gradient

solutions. Therefore, the presented numerical method can be validated here to numerically investigate the effect of the quadratic pressure gradient term on such moving boundary problems.

5 Results and discussions

5.1 Significance of considering quadratic pressure gradient term

According to the general values of the physical parameters, the value of the dimensionless compressibility α_D is estimated to be in the range of 0.0001–0.01 [55,56]. In terms of the definition of dimensionless compressibility, the low rock permeability in low-permeability reservoirs or the high viscosity of fluid in heavy-oil reservoirs can lead to a higher value of dimensionless compressibility, in contrast with conventional reservoirs. Here, without loss of generality, α_D is set to 0.008.

To compare with the effect of the quadratic pressure gradient term on the Darcy flow models, the exact analytical solution for a one-dimensional Darcy's flow problem ($\lambda_D = 0$), without considering the quadratic pressure gradient term [10], as follows

$$P_D(x_D, t_D) = -x_D + 2\sqrt{\frac{t_D}{\pi}}\exp\left(-\frac{x_D^2}{4t_D}\right) + x_D \mathrm{erf}\left(\frac{x_D}{2\sqrt{t_D}}\right), x_D \in [0, \infty]. \quad (53)$$

Moreover, through the inverse Laplace transform [66–68], the exact analytical solution for the same Darcy's flow problem, but considering the quadratic pressure gradient term, can also be obtained as follows (Appendix 2)

$$P_D(x_D, t_D) = -\frac{1}{\alpha_D}\cdot \ln\left[\exp\left(\alpha_D \cdot x_D + \alpha_D^2 \cdot t_D\right) \cdot \mathrm{erfc}\left(\alpha_D \cdot \sqrt{t_D} + \frac{x_D}{2\sqrt{t_D}}\right) - \mathrm{erfc}\left(\frac{x_D}{2\sqrt{t_D}}\right) + 1\right], \quad x_D \in [0, \infty]. \quad (54)$$

From Eqs. (53) and (54), the relative error function $\varepsilon_r(x_D, t_D)$ of the dimensionless formation pressure for the one-dimensional Darcy's flow can be formulated, caused by neglecting the nonlinear quadratic pressure gradient term, as follows

$$\varepsilon_r(x_D, t_D) = \frac{\left| -x_D + 2\sqrt{\frac{t_D}{\pi}} \exp\left(-\frac{x_D^2}{4t_D}\right) + x_D \mathrm{erf}\left(\frac{x_D}{2\sqrt{t_D}}\right) + \frac{1}{\alpha_D} \cdot \ln\left[\exp\left(\alpha_D \cdot x_D + \alpha_D^2 \cdot t_D\right) \cdot \mathrm{erfc}\left(\alpha_D \cdot \sqrt{t_D} + \frac{x_D}{2\sqrt{t_D}}\right) - \mathrm{erfc}\left(\frac{x_D}{2\sqrt{t_D}}\right) + 1\right] \right|}{\left| \frac{1}{\alpha_D} \cdot \ln\left[\exp\left(\alpha_D \cdot x_D + \alpha_D^2 \cdot t_D\right) \cdot \mathrm{erfc}\left(\alpha_D \cdot \sqrt{t_D} + \frac{x_D}{2\sqrt{t_D}}\right) - \mathrm{erfc}\left(\frac{x_D}{2\sqrt{t_D}}\right) + 1\right] \right|} \times 100\,\%. \tag{55}$$

Using the numerical tests in the MATLAB software package from Eq. (55), it can be established that for a range of dimensionless time [0, 10000] and a range of dimensionless distance [0, 300], the relative error of the formation pressure, caused by neglecting the quadratic pressure gradient term, can be controlled to no more than 5 % by setting the value of the dimensionless compressibility α_D to no more than 0.00095 (Fig. 6). Furthermore, from Fig. 6 it can be shown that for Darcy's flow, the greater the dimensionless time, the larger the relative error from neglecting the quadratic pressure gradient term; but for an arbitrary dimensionless time, there exists a maximum value for the relative error function with respect to the dimensionless distance; before the dimensionless distance corresponding to the maximum value, the relative error increases as the dimensionless distance increases, whereas after the dimensionless distance, the relative error decreases as the dimensionless distance increases; the greater the dimensionless time, the larger the dimensionless distance, which corresponds to the maximum relative error of the dimensionless formation pressure.

However, for the moving boundary model (the dimensionless threshold pressure gradient λ_D is set to 0.852 based on actual experimental data) with a critical value of α_D = 0.00095, the relative error will largely exceed the tolerated relative errors by 5 % for engineering applications. Figures 7 and 8 show the numerically computed relative errors of the dimensionless formation pressure when t_D = 10000 and the dimensionless transient wellbore pressure, caused by neglecting the quadratic pressure gradient term. From Fig. 7

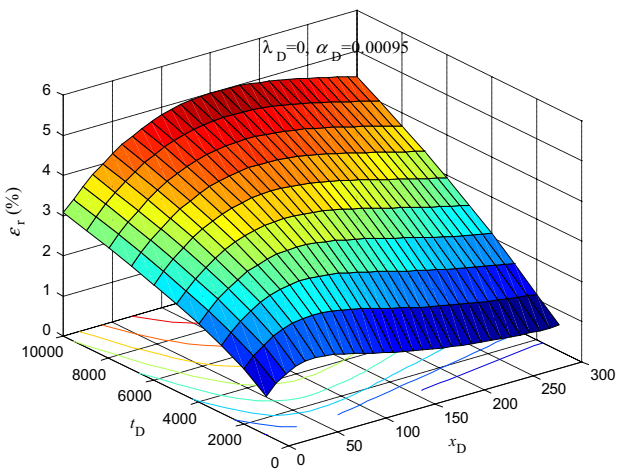

Fig. 6 Relative error surface of analytically solved dimensionless formation pressure for one-dimensional Darcy's flow as a result of neglecting quadratic pressure gradient term

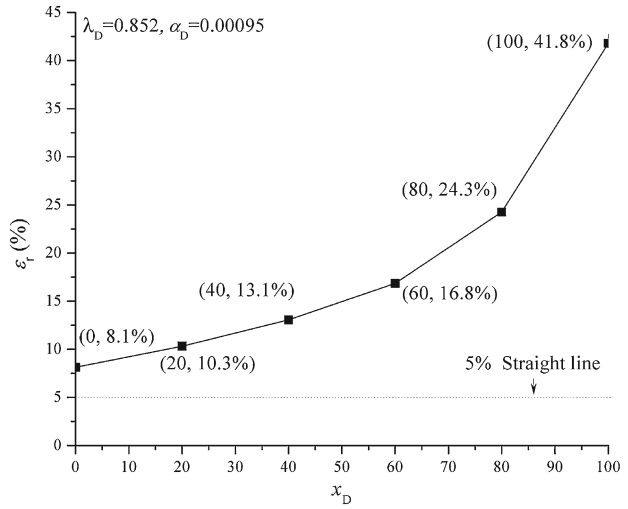

Fig. 7 Relative error curves of numerically solved dimensionless formation pressure distribution when t_D = 10000 for one-dimensional seepage flow with threshold pressure gradient as a result of neglecting the quadratic pressure gradient term

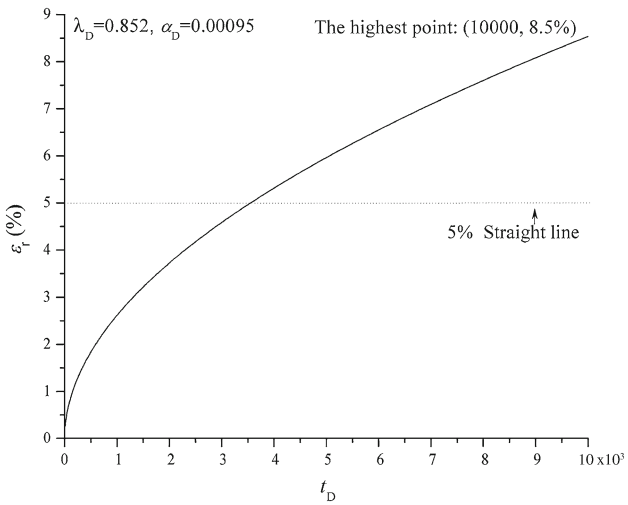

Fig. 8 Relative error curves of numerically solved dimensionless transient wellbore pressure for one-dimensional seepage flow with threshold pressure gradient as a result of neglecting quadratic pressure gradient term

it can be seen that the relative errors of the dimensionless formation pressure for the entire disturbed distance from the well are larger than 5 %; moreover, the larger the dimensionless distance, the larger the relative errors; the largest relative error can reach as high as 41.8 %, for this case in Fig. 7. From Fig. 8 it can be seen that initially, the relative error of the dimensionless transient wellbore pressure is less than 5 %; however, as the dimensionless time increases, the relative error may exceed 5 % following a production period; the greater the dimensionless time, the larger the relative error; the largest error can reach as high as 8.5 % when $t_D = 10000$.

In conclusion, although the effect of the quadratic pressure gradient term can be neglected for a one-dimensional Darcy's flow problem when the value of the dimensionless compressibility is set to no more than the critical value ($\alpha_D = 0.00095$), the effect of this quadratic pressure gradient term may not be neglected for seepage flow with a threshold pressure gradient having the same value of the dimensionless compressibility.

5.2 Effect of quadratic pressure gradient term under different values of threshold pressure gradient

Figures 9 and 10 show the effect of the quadratic pressure gradient term on the dimensionless formation pressure distribution and dimensionless transient wellbore pressure with different values of the dimensionless threshold pressure gradient. From Figs. 9 and 10, it can be seen that the effect of the quadratic pressure gradient term on the dimensionless formation pressure distribution and dimensionless transient wellbore pressure becomes increasingly obvious as the dimensionless threshold pressure gradient increases.

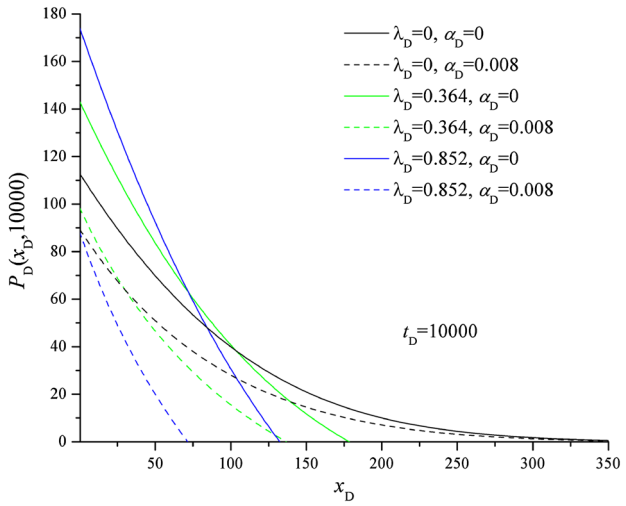

Fig. 9 Effect of quadratic pressure gradient term on dimensionless formation pressure distribution with different values of dimensionless threshold pressure gradient

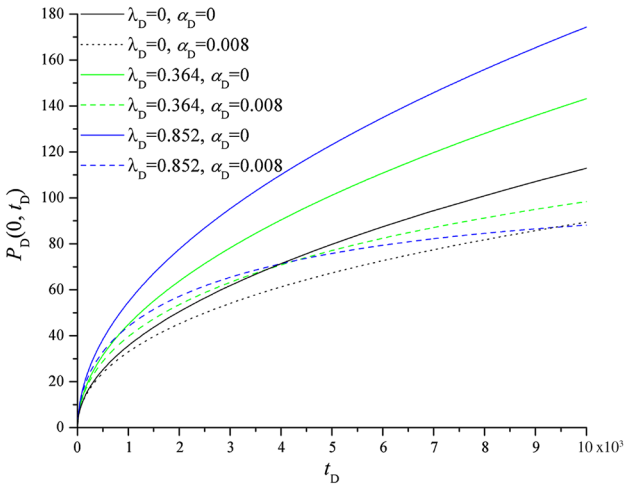

Fig. 10 Effect of quadratic pressure gradient term on dimensionless transient wellbore pressure with different values of dimensionless threshold pressure gradient

Figure 10 indicates the effects of the quadratic pressure gradient term on the dimensionless transient wellbore pressure. The larger the dimensionless threshold pressure gradient, the larger the dimensionless transient wellbore pressure if the quadratic pressure gradient term is neglected, while the curves of the dimensionless transient wellbore pressure corresponding to different values of the dimensionless threshold pressure gradient may have intersection points (except for the origin point) in the large dimensionless time if the quadratic pressure gradient term is considered.

Tables 2 and 3 show a comparison between the two cases considering and not considering the quadratic pressure gradient terms for the already computed dimensionless formation pressure distribution and dimensionless transient wellbore pressure with different values of the dimensionless threshold pressure gradient. They also include the corresponding relative errors; the relative error ε_r is equal to the absolute error divided by the magnitude of the exact value, i.e., $|P_{D2} - P_{D1}|/P_{D1}$ in this problem, where P_{D1} denotes the solutions of the models considering the quadratic pressure gradient term, and P_{D2} denotes those without considering the quadratic pressure gradient term. The relative error curves are plotted in Figs. 11 and 12 using the data from Tables 2 and 3, respectively.

From Tables 2 and 3, it can be concluded that the greatest relative error for the computed dimensionless formation pressure, from neglecting the quadratic pressure gradient term, can reach as high as 677.59 % when $\lambda_D = 0.852$; and the greatest relative error for the computed dimensionless transient wellbore pressure can reach as high as 94.89 % when $\lambda_D = 0.852$. Figures 11 and 12 show clearly that for any case with the same value of the dimensionless threshold pressure gradient ($\lambda_D > 0$), the greater the dimensionless distance,

Table 2 Comparison data for computed dimensionless formation pressure distribution and relative errors

t_D	$\lambda_D = 0.852$			$\lambda_D = 0.364$			$\lambda_D = 0$		
	P_{D1} ($\alpha_D = 0.008$)	P_{D2} ($\alpha_D = 0$)	ε_r (%)	P_{D1} ($\alpha_D = 0.008$)	P_{D2} ($\alpha_D = 0$)	ε_r (%)	P_{D1} ($\alpha_D = 0.008$)	P_{D2} ($\alpha_D = 0$)	ε_r (%)
Computed dimensionless transient wellbore pressure P_D (0, t_D)									
1000	44	54.67	24.25	39.65	44.96	13.39	32.97	35.68	8.22
2000	57.16	77.63	35.81	53.54	63.82	19.20	45.2	50.46	11.64
3000	65.44	95.29	45.61	63.23	78.22	23.71	54.08	61.8	14.28
4000	71.32	110.06	54.32	70.8	90.44	27.74	61.25	71.36	16.51
5000	75.81	123.14	62.43	77.07	101.16	31.26	67.34	79.79	18.49
6000	79.33	134.89	70.04	82.35	110.85	34.61	72.67	87.4	20.27
7000	82.23	145.8	77.31	87.07	119.77	37.56	77.44	94.41	21.91
8000	84.62	155.96	84.31	91.2	128.03	40.38	81.77	100.93	23.43
9000	86.56	165.32	90.99	95.02	135.85	42.97	85.73	107.05	24.87
10000	89.41	174.25	94.89	98.46	143.15	45.39	89.4	112.84	26.22

Table 3 Comparison data for computed dimensionless transient wellbore pressure and relative errors

x_D	$\lambda_D = 0.852$			$\lambda_D = 0.364$			$\lambda_D = 0$		
	P_6 ($\alpha_D = 0.008$)	P_{D2} ($\alpha_D = 0$)	ε_r (%)	P_{D1} ($\alpha_D = 0.008$)	P_{D2} ($\alpha_D = 0$)	ε_6 (%)	P_{D1} ($\alpha_D = 0.008$)	P_{D2} ($\alpha_D = 0$)	ε_r (%)
Computed dimensionless formation pressure distribution P_D (x_D, 10000)									
0	87.59	173.66	98.26	98.19	142.85	45.48	89.4	112.84	26.22
20	55.98	139.63	149.43	74.09	117.36	58.40	71.49	93.96	31.43
40	31.1	106.74	243.22	54.67	94.06	72.05	57.06	77.32	35.51
60	10.13	78.77	677.59	39.14	73.58	87.99	45.34	62.84	38.60
80	0	52.85	*	26.18	56.22	114.74	35.8	50.43	40.87
100	0	30.85	*	15.56	40.69	161.50	28.04	39.93	42.40
120	0	11.16	*	6.49	27.73	327.27	21.77	31.19	43.27
140	0	0	*	0	16.59	*	16.72	24.02	43.66
160	0	0	*	0	7.52	*	12.69	18.23	43.66
180	0	0	*	0	0	*	9.52	13.64	43.28
200	0	0	*	0	0	*	7.05	10.05	42.55

* denotes the null data

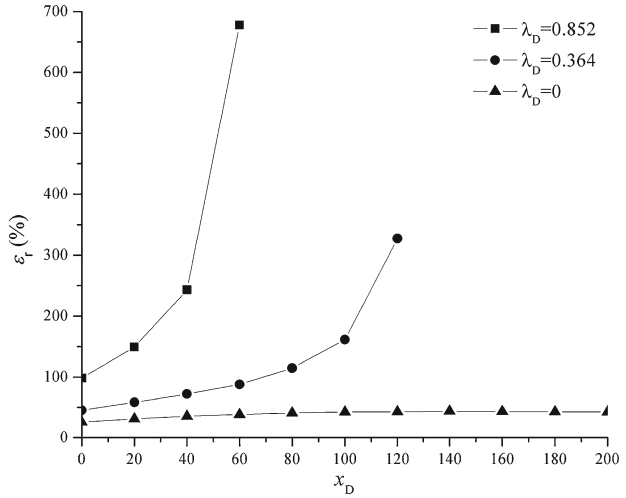

Fig. 11 Relative error curves for computing dimensionless formation pressure distribution as a result of neglecting quadratic pressure gradient term, with different values of dimensionless threshold pressure gradient

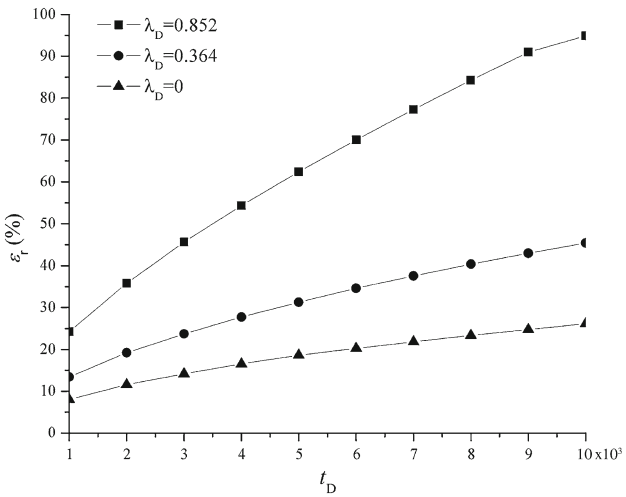

Fig. 12 Relative error curves for computing dimensionless transient wellbore pressure as a result of neglecting quadratic pressure gradient term, with different values of dimensionless threshold pressure gradient

the larger the relative error of the dimensionless formation pressure; and the larger the dimensionless time, the larger the relative error of the dimensionless transient wellbore pressure, especially for the case corresponding to the largest value of the dimensionless threshold pressure gradient, $\lambda_D = 0.852$. The growth of relative errors, as the dimensionless distance from the wellbore or the dimensionless time increases, can be accelerated by the threshold pressure gradient. The relative errors corresponding to Darcy's law remain at a lower level, and the change in the relative error of the dimensionless formation pressure with the dimensionless distance increasing is not very obvious, whereas the relative error of the dimensionless transient wellbore pressure still clearly increases as the dimensionless time increases.

In conclusion, the quadratic pressure gradient term has a significant effect on the mathematical model solutions of seepage flow with a dimensionless threshold pressure gradient ($\lambda_D > 0$) with respect to the dimensionless formation pressure, dimensionless transient wellbore pressure, and dimensionless transient distance of the moving boundary; the greater the dimensionless distance from the wellbore, the greater the effect of the quadratic pressure gradient term on the dimensionless formation pressure; the greater the dimensionless time, the greater the effect of the quadratic pressure gradient term on the dimensionless transient wellbore pressure. In summary, compared with classical Darcy's flow models, the moving boundary models of seepage flow with a threshold pressure gradient should more necessarily take into account the quadratic pressure gradient term.

5.3 Sensitive effect of quadratic pressure gradient term

Figures 13, 14, and 15 show the sensitive effect of the quadratic pressure gradient term on the formation pressure distribution, transient wellbore pressure, and transient distance of the moving boundary, respectively, given a certain value of dimensionless threshold pressure gradient. Figures 13, 14, and 15 show that larger values of the dimensionless compressibility α_D correspond to smaller values of the dimensionless formation pressure, dimensionless transient wellbore pressure, and dimensionless transient distance of the moving boundary. What's more, the sensitive effects of the quadratic pressure gradient term on the formation pressure distribution, the transient wellbore pressure, and the transient distance of the moving boundary tend to diminish as the dimensionless threshold pressure gradient increases for the one-dimensional problem.

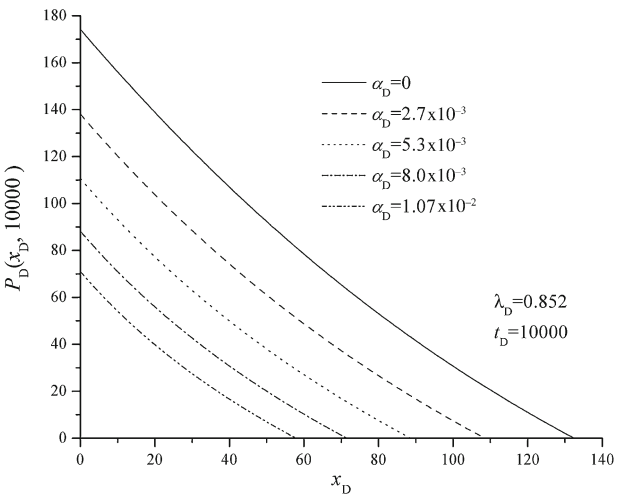

Fig. 13 Sensitive effect of quadratic pressure gradient term on dimensionless formation pressure distribution

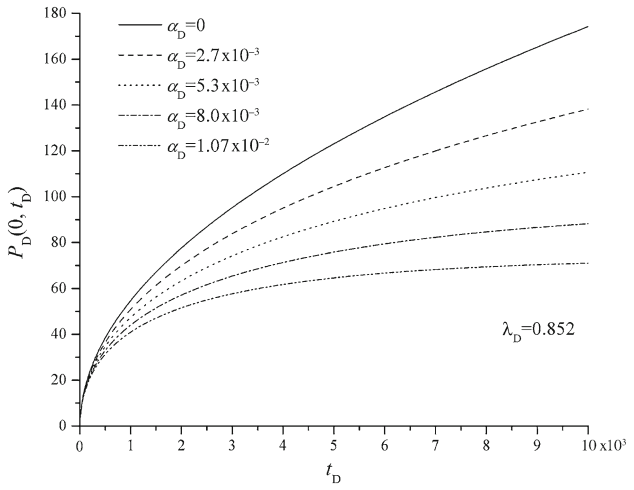

Fig. 14 Sensitive effect of quadratic pressure gradient term on dimensionless transient wellbore pressure

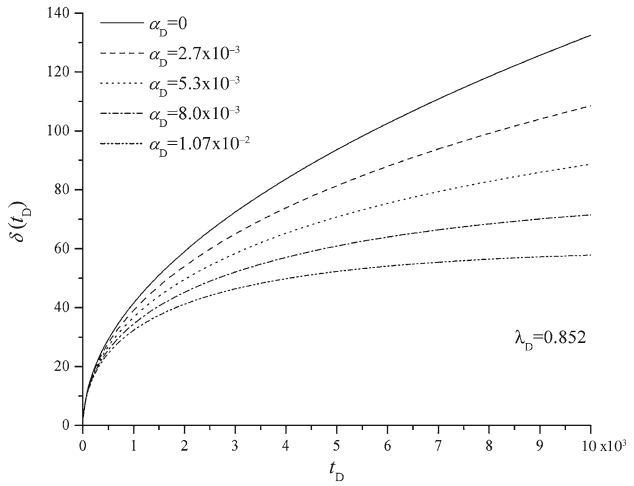

Fig. 15 Sensitive effect of quadratic pressure gradient term on dimensionless transient distance of moving boundary

6 Conclusions

A moving boundary problem of one-dimensional seepage flow with a threshold pressure gradient, considering the quadratic pressure gradient term, is built. And a verified numerical method is applied to solve the nonlinear problem. Numerical result analysis shows that, in contrast to a Darcy's flow problem, it is more necessary to take into account the quadratic pressure gradient terms in the relevant governing equations for problems of seepage flow with a threshold pressure gradient. Moreover, the sensitive effects of the quadratic pressure gradient term on numerical solutions tend to diminish as the dimensionless threshold pressure gradient increases for the one-dimensional problem.

Acknowledgments The authors would like to acknowledge the funding by the project (Grant 51404232) sponsored by the National Natural Science Foundation of China, the National Science and Technology Major Project (Grant 2011ZX05038003), and the China Postdoctoral Science Foundation project (Grant 2014M561074). In particular, Wenchao Liu would also like to express his deepest gratitude to the China Scholarship Council for its generous financial support of the research. Special thanks go to Dr. Yongfei Yang, Dr. Lili Xue, and Dr. Lei Zhang for their tremendous help in improving the writing and wording of the paper.

Appendix 1

Equation (1) can be rewritten as follows

$$p = \frac{1}{C_f} \ln \rho - \frac{1}{C_f} \ln \rho_0 + p_0. \tag{56}$$

Differentiating the two sides of Eq. (56) with respect to x, we have

$$\frac{\partial p}{\partial x} = \frac{1}{C_f \cdot \rho} \frac{\partial \rho}{\partial x}, \tag{57}$$

Equation (57) can be rewritten as follows

$$\frac{\partial \rho}{\partial x} = C_f \cdot \rho \frac{\partial p}{\partial x}, \tag{58}$$

In the same manner as previously, from Eqs. (1) and (2) the following equations can also be deduced:

$$\frac{\partial \rho}{\partial t} = C_f \cdot \rho \frac{\partial p}{\partial t}, \tag{59}$$

$$\frac{\partial \phi}{\partial t} = C_\phi \cdot \phi \frac{\partial p}{\partial t}. \tag{60}$$

The left-hand side of Eq. (4) can be expanded as follows

$$-\frac{\partial}{\partial x}(\rho \cdot \upsilon) = \frac{k}{\mu} \cdot \rho \cdot \frac{\partial^2 p}{\partial x^2} + \frac{k}{\mu} \cdot \frac{\partial \rho}{\partial x} \cdot \frac{\partial p}{\partial x} - \frac{k \cdot \lambda \cdot C_f}{\mu} \cdot \rho \cdot \frac{\partial p}{\partial x}, \tag{61}$$

Substituting Eq. (58) into the right-hand side of Eq. (61) yields

$$-\frac{\partial}{\partial x}(\rho \cdot \upsilon) = \underbrace{\frac{k}{\mu} \cdot \rho \cdot \frac{\partial^2 p}{\partial x^2}}_{\text{Main Term}} + \underbrace{\frac{k \cdot C_f}{\mu} \cdot \rho \cdot \left(\frac{\partial p}{\partial x}\right)^2}_{\text{Quadratic Gradient Term}} \underbrace{- \frac{k \cdot \lambda \cdot C_f}{\mu} \cdot \rho \cdot \frac{\partial p}{\partial x}}_{\text{Small Term}}, \tag{62}$$

Because $\lambda << 1$, and $C_f << 1$, the small term on the right-hand side of Eq. (62) can be neglected, and then Eq. (62) can be rewritten as follows

$$-\frac{\partial}{\partial x}(\rho\cdot\upsilon)=\underbrace{\frac{k}{\mu}\cdot\rho\cdot\frac{\partial^2 p}{\partial x^2}}_{\text{Main Term}}+\underbrace{\frac{k\cdot C_{\mathrm{f}}}{\mu}\cdot\rho\cdot\left(\frac{\partial p}{\partial x}\right)^2}_{\text{Quadratic Gradient Term}}, \tag{63}$$

In Eq. (63), the quadratic pressure gradient term is retained for the deduction of the governing equation.

Expanding the right-hand side of Eq. (4) yields

$$\frac{\partial(\rho\phi)}{\partial t}=\rho\frac{\partial\phi}{\partial t}+\phi\frac{\partial\rho}{\partial t}, \tag{64}$$

Substituting Eqs. (59) and (60) into the right-hand side of Eq. (64) yields

$$\begin{aligned}\frac{\partial(\rho\phi)}{\partial t}&=\rho\cdot C_\phi\cdot\phi\cdot\frac{\partial p}{\partial t}+\phi\cdot C_{\mathrm{f}}\cdot\rho\cdot\frac{\partial p}{\partial t}\\&=\rho\cdot\phi\cdot\frac{\partial p}{\partial t}\cdot\left(C_\phi+C_{\mathrm{f}}\right)=\rho\cdot\phi\cdot\frac{\partial p}{\partial t}\cdot C_{\mathrm{t}}.\end{aligned} \tag{65}$$

Substituting Eqs. (63) and (65) into Eq. (4), the governing equation in consideration of the quadratic pressure gradient term can be obtained as follows

$$\underbrace{\frac{k}{\mu}\cdot\rho\cdot\frac{\partial^2 p}{\partial x^2}}_{\text{Main Term}}+\underbrace{\frac{k\cdot C_{\mathrm{f}}}{\mu}\cdot\rho\cdot\left(\frac{\partial p}{\partial x}\right)^2}_{\text{Quadratic Gradient Term}}=\rho\cdot\phi\cdot\frac{\partial p}{\partial t}\cdot C_{\mathrm{t}}. \tag{66}$$

Equation (66) can be equivalently simplified, by canceling the variable ρ on both sides, as follows

$$\frac{k}{\mu}\cdot\frac{\partial^2 p}{\partial x^2}+\frac{k\cdot C_{\mathrm{f}}}{\mu}\cdot\left(\frac{\partial p}{\partial x}\right)^2=\phi\cdot\frac{\partial p}{\partial t}\cdot C_{\mathrm{t}}. \tag{67}$$

Appendix 2

The dimensionless mathematical model, considering the quadratic threshold pressure gradient, for the one-dimensional Darcy's flow in semi-infinite long porous media for the case of a constant flow rate at the inner boundary is as follows

$$\frac{\partial^2 P_{\mathrm{D}}}{\partial x_{\mathrm{D}}^2}-\alpha_{\mathrm{D}}\left(\frac{\partial P_{\mathrm{D}}}{\partial x_{\mathrm{D}}}\right)^2=\frac{\partial P_{\mathrm{D}}}{\partial t_{\mathrm{D}}}, \tag{68}$$

$$P_{\mathrm{D}}|_{t_{\mathrm{D}}=0}=0, \tag{69}$$

$$\left.\frac{\partial P_{\mathrm{D}}}{\partial x_{\mathrm{D}}}\right|_{x_{\mathrm{D}}=0}=-1, \tag{70}$$

$$P_{\mathrm{D}}|_{x_{\mathrm{D}}\to\infty}=0. \tag{71}$$

First, introduce the following transform [52]:

$$P_{\mathrm{D}}=-\frac{1}{\alpha_{\mathrm{D}}}\cdot\ln U. \tag{72}$$

Substituting Eq. (72) into Eqs. (68)–(71) yields

$$\frac{\partial^2 U}{\partial x_{\mathrm{D}}^2}=\frac{\partial U}{\partial t_{\mathrm{D}}}, \tag{73}$$

$$U|_{t_{\mathrm{D}}=0}=1, \tag{74}$$

$$\left.\frac{\partial U}{\partial x_{\mathrm{D}}}\right|_{x_{\mathrm{D}}=0}=\alpha_{\mathrm{D}}\cdot U|_{x_{\mathrm{D}}=0}, \tag{75}$$

$$U|_{x_{\mathrm{D}}\to\infty}=1. \tag{76}$$

By the linear Laplace transform,

$$\ell[U]=\int_0^\infty U\cdot\exp\left(-s\cdot t_{\mathrm{D}}\right)\mathrm{d}t_{\mathrm{D}}. \tag{77}$$

Equations (73)–(76) can be transformed as

$$\frac{\partial^2\ell[U]}{\partial x_{\mathrm{D}}^2}=s\ell[U]-1, \tag{78}$$

$$\left.\frac{\partial\ell[U]}{\partial x_{\mathrm{D}}}\right|_{x_{\mathrm{D}}=0}=\alpha_{\mathrm{D}}\cdot\ell[U]|_{x_{\mathrm{D}}=0}, \tag{79}$$

$$\ell[U]|_{x_{\mathrm{D}}\to\infty}=\frac{1}{s}. \tag{80}$$

The analytical solution for Eqs. (78)–(80) can be solved as follows [52]

$$\ell[U]=-\frac{\alpha_{\mathrm{D}}\cdot\exp\left(-x_{\mathrm{D}}\sqrt{s}\right)}{\left(\alpha_{\mathrm{D}}+\sqrt{s}\right)s}+\frac{1}{s}. \tag{81}$$

The following Laplace and inverse Laplace transforms are known [66–68] as

$$\ell^{-1}\left[\frac{1}{s}\right]=1, \tag{82}$$

$$\begin{aligned}&\ell^{-1}\left[\frac{\alpha_{\mathrm{D}}\cdot\exp\left(-x_{\mathrm{D}}\sqrt{s}\right)}{\left(\alpha_{\mathrm{D}}+\sqrt{s}\right)s}\right]\\&=-\exp\left(\alpha_{\mathrm{D}}\cdot x_{\mathrm{D}}+\alpha_{\mathrm{D}}^2\cdot t_{\mathrm{D}}\right)\operatorname{erfc}\left(\alpha_{\mathrm{D}}\sqrt{t_{\mathrm{D}}}+\frac{x_{\mathrm{D}}}{2\sqrt{t_{\mathrm{D}}}}\right)\\&\quad+\operatorname{erfc}\left(\frac{x_{\mathrm{D}}}{2\sqrt{t_{\mathrm{D}}}}\right).\end{aligned} \tag{83}$$

Therefore, from Eq. (81), we obtain

$$\begin{aligned}U=&\exp\left(\alpha_{\mathrm{D}}\cdot x_{\mathrm{D}}+\alpha_{\mathrm{D}}^2\cdot t_{\mathrm{D}}\right)\operatorname{erfc}\left(\alpha_{\mathrm{D}}\sqrt{t_{\mathrm{D}}}+\frac{x_{\mathrm{D}}}{2\sqrt{t_{\mathrm{D}}}}\right)\\&+\operatorname{erfc}\left(\frac{x_{\mathrm{D}}}{2\sqrt{t_{\mathrm{D}}}}\right)+1.\end{aligned} \tag{84}$$

Then, substituting Eq. (84) into Eq. (72), we obtain the exact analytical solution of P_D as follows

$$P_D = -\frac{1}{\alpha_D} \cdot \ln \left[\exp\left(\alpha_D \cdot x_D + \alpha_D^2 \cdot t_D\right) \times \operatorname{erfc}\left(\alpha_D \sqrt{t_D} + \frac{x_D}{2\sqrt{t_D}}\right) + \operatorname{erfc}\left(\frac{x_D}{2\sqrt{t_D}}\right) + 1 \right]. \tag{85}$$

References

1. Huang, Y.Z., Yang, Z.M., He, Y., et al.: An overview on nonlinear porous flow in low permeability porous Media. Theor. Appl. Mech. Lett. **3**, 022001 (2013)
2. Monteiro, P.J.M., Rycroft, C.H., Barenblatt, G.I.: A mathematical model of fluid and gas flow in nanoporous media. Proc. Natl. Acad. Sci. USA **109**, 20309–20313 (2012)
3. Balhoff, M., Sanchez-Rivera, D., Kwok, A., et al.: Numerical algorithms for network modeling of yield stress and other non-Newtonian fluids in porous media. Transp. Porous Media **93**, 363–379 (2012)
4. Yu, R.Z., Bian, Y.N., Li, Y., et al.: Non-Darcy flow numerical simulation of XPJ low permeability reservoir. J. Pet. Sci. Eng. **92–93**, 40–47 (2012)
5. Yu, R.Z., Bian, Y.N., Zhou, S., et al.: Nonlinear flow numerical simulation of low-permeability reservoir. J. Cent. South Univ. Technol. **19**, 1980–1987 (2012)
6. Guo, J.J., Zhang, S., Zhang, L.H., et al.: Well testing analysis for horizontal well with consideration of threshold pressure gradient in tight gas reservoirs. J. Hydrodyn. **24**, 561–568 (2012)
7. Luo, W.J., Wang, X.D.: Effect of a moving boundary on the fluid transient flow in low permeability Reservoirs. J. Hydrodyn. **24**, 391–398 (2012)
8. Yao, J., Liu, W.C., Chen, Z.X.: Numerical solution of a moving boundary problem of one-dimensional flow in semi-infinite long porous media with threshold pressure gradient. Math. Probl. Eng. **2013**, 384246 (2013)
9. Zeng, B.Q., Cheng, L.S., Li, C.L.: Low velocity non-linear flow in ultra-low permeability reservoir. J. Pet. Sci. Eng. **80**, 1–6 (2012)
10. Liu, W.C., Yao, J., Wang, Y.Y.: Exact analytical solutions of moving boundary problems of one-dimensional flow in semi-infinite long porous media with threshold pressure gradient. Int. J. Heat Mass Transf. **55**, 6017–6022 (2012)
11. Liu, W.C., Yao, J., Chen, Z.X., et al.: Analytical solution of a double moving boundary problem for nonlinear flows in one-dimensional semi-infinite long porous media with low permeability. Acta Mech. Sin. **30**, 50–58 (2014)
12. Zhu, W.Y., Song, H.Q., Huang, X.H., et al.: Pressure characteristics and effective deployment in a water—bearing tight gas reservoir with low-velocity non-Darcy flow. Energy Fuels **25**, 1111–1117 (2011)
13. Beygi, M.E., Rashidi, F.: Analytical solutions to gas flow problems in low permeability porous media. Transp. Porous Media **87**, 421–436 (2011)
14. Cai, J.C., Yu, B.M.: A discussion of the effect of tortuosity on the capillary imbibition in porous media. Transp. Porous Media **89**, 251–263 (2011)
15. Wang, X.W., Yang, Z.M., Qi, Y.D., et al.: Effect of absorption boundary layer on nonlinear flow in low permeability porous media. J. Cent. South Univ. Technol. **18**, 1299–1303 (2011)
16. Jing, W., Liu, H.Q., Pang, Z.X., et al.: The investigation of threshold pressure gradient of foam flooding in porous media. Pet. Sci. Technol. **29**, 2460–2470 (2011)
17. Xu, Q.Y., Liu, X.G., Yang, Z.M., et al.: The model and algorithm of a new numerical simulation software for low permeability reservoirs. J. Pet. Sci. Eng. **78**, 239–242 (2011)
18. Yao, Y.D., Ge, J.L.: Characteristics of non-Darcy flow in low-permeability reservoirs. Pet. Sci. **8**, 55–62 (2011)
19. Civan, F.: Porous Media Transport Phenomena. JohnWiley & Sons Press, Inc, Hoboken (2011)
20. Song, F.Q., Wang, J.D., Liu, H.L.: Static threshold pressure gradient characteristics of liquid influenced by boundary wettability. Chin. Phys. Lett. **27**, 024704 (2010)
21. Daprà, I., Scarpi, G.: Unsteady simple shear flow in a viscoplastic fluid: comparison between analytical and numerical solutions. Rheol. Acta **49**, 15–22 (2010)
22. Xie, K.H., Wang, K., Wang, Y.L., et al.: Analytical solution for one-dimensional consolidation of clayey soils with a threshold gradient. Comput. Geotech. **37**, 487–493 (2010)
23. Yue, X.A., Wei, H.G., Zhang, L.J., et al.: Low pressure gas percolation characteristic in ultra-low permeability porous media. Transp. Porous Media **85**, 333–345 (2010)
24. Yun, M.J., Yu, B.M., Lu, J.D., et al.: Fractal analysis of Herschel-Bulkley fluid flow in porous media. Int. J. Heat Mass Transf. **53**, 3570–3574 (2010)
25. Li, Y., Yu, B.M.: Study of the starting pressure gradient in branching network. Sci. China Technol. Sci. **53**, 2397–2403 (2010)
26. Zhao, Y.S., Kumar, L., Paso, K., et al.: Gelation behavior of model wax-oil and crude oil systems and yield stress model development. Energy Fuels **26**, 6323–6331 (2012)
27. Fossen, M., Øyangen, T., Velle, O.J.: Effect of the pipe diameter on the restart pressure of a gelled waxy crude oil. Energy Fuels **27**, 3685–3691 (2013)
28. Papanastasiou, T.C., Boudouvis, A.G.: Flows of viscoplastic materials: models and computation. Comput. Struct. **64**, 677–694 (1997)
29. Prada, A., Civan, F.: Modification of Darcy's law for the threshold pressure gradient. J. Pet. Sci. Eng. **22**, 237–240 (1999)
30. Nedoma, J.: Numerical solution of a Stefan-like problem in Bingham rheology. Math. Comput. Simul. **61**, 271–281 (2003)
31. Chen, M., William, R., Yannis, C.Y.: The flow and displacement in porous media of fluids with yield stress. Chem. Eng. Sci. **60**, 4183–4202 (2005)
32. Wang, S.J., Huang, Y.Z., Civan, F.: Experimental and theoretical investigation of the Zaoyuan field heavy oil flow through porous media. J. Pet. Sci. Eng. **50**, 83–101 (2006)
33. Song, F.Q., Jiang, R.J., Bian, S.L.: Measurement of threshold pressure gradient of microchannels by static Method. Chin. Phys. Lett. **24**, 1995–1998 (2007)
34. Hao, F., Cheng, L.S., Hassan, O., et al.: Threshold pressure gradient in ultra-low permeability reservoirs. Pet. Sci. Technol. **26**, 1024–1035 (2008)
35. Yun, M.J., Yu, B.M., Cai, J.C.: A fractal model for the starting pressure gradient for Bingham fluids in porous media. Int. J. Heat Mass Transf. **51**, 1402–1408 (2008)
36. Wang, F., Yue, X.A., Xu, S.L., et al.: Influence of wettability on flow characteristics of water through microtubes and cores. Chin. Sci. Bull. **54**, 2256–2262 (2009)
37. Xiong, W., Lei, Q., Gao, S.S., et al.: Pseudo threshold pressure gradient to flow for low permeability reservoirs. Pet. Explor. Dev. **36**, 232–236 (2009)
38. Cai, J.C., Yu, B.M., Zou, M.Q., et al.: Fractal analysis of invasion depth of extraneous fluids in porous Media. Chem. Eng. Sci. **65**, 5178–5186 (2010)
39. Cai, J.C., Hu, X.Y., Standnes, D.C., et al.: An analytical model for spontaneous imbibition in fractal porous media including gravity. Coll. Surf. A **414**, 228–323 (2012)

40. Darcy, H.: Les Fontaines Publiques de La Ville de Dijon [The Public Fountains of the Town of Dijon]. Dalmont, Paris (1856) (in French)
41. Cai, J.C.: A fractal approach to low velocity non-Darcy flow in a low permeability porous medium. Chin. Phys. B **23**, 044701 (2014)
42. Pascal, H.: Nonsteady flow through porous media in the presence of a threshold pressure gradient. Acta Mech. **39**, 207–224 (1981)
43. Wu, Y.S., Pruess, K., Witherspoon, P.A.: Flow and displacement of Bingham non-Newtonian fluids in porous Media. SPE Reserv. Eng. **7**, 369–376 (1992)
44. Song, F.Q., Liu, C.Q., Li, F.H.: Transient pressure of percolation through one dimension porous media with threshold pressure gradient. Appl. Math. Mech. **20**, 27–35 (1999)
45. Zhu, Y., Xie, J.Z., Yang, W.H., et al.: Method for improving history matching precision of reservoir numerical simulation. Pet. Explor. Dev. **35**, 225–229 (2008)
46. Feng, G.Q., Liu, Q.G., Shi, G.Z., et al.: An unsteady seepage flow model considering kickoff pressure gradient for low-permeability gas reservoirs. Pet. Explor. Dev. **35**, 457–461 (2008)
47. Marshall, S.L.: Nonlinear pressure diffusion in flow of compressible liquids through porous media. Transp. Porous Media **77**, 431–446 (2009)
48. Bai, M., Ma, Q.G., Roegiers, J.C.: A nonlinear dual-porosity model. Appl. Math. Modell. **18**, 602–610 (1994)
49. Cao, X.L., Tong, D.K., Wang, R.H.: Exact solutions for nonlinear transient flow model including a quadratic gradient term. Appl. Math. Mech. **25**, 102–109 (2004)
50. Tong, D.K., Zhang, H.Q., Wang, R.H.: Exact solution and its behavior characteristic of nonlinear dual-porosity model. Appl. Math. Mech. **26**, 1277–1283 (2005)
51. Chakrabarty, C., Farouq, A.S.M., Tortike, W.S.: Effects of the nonlinear gradient term on the transient pressure solution for a radial flow system. J. Pet. Sci. Eng. **8**, 241–256 (1993)
52. Odeh, A.S., Babu, D.K.: Comparison of solutions of the nonlinear and linearized diffusion equations. SPE Reserv. Eng. **3**, 1202–1206 (1988)
53. Finjord, J., Aadnoy, B.S., Rogaland, R.C.: Effects of the quadratic gradient term in steady-state and semisteady-state solutions for reservoir pressure. SPE Form. Eval. **4**, 413–417 (1989)
54. Wang, Y., Dusseault, M.B.: The effect of quadratic gradient terms on the borehole solution in poroelastic Media. Water Resour. Res. **27**, 3215–3223 (1991)
55. Chakrabarty, C., Farouq, A.S.M., Tortike, W.S.: Analytical solutions for radial pressure distribution including the effects of the quadratic-gradient term. Water Resour. Res. **29**, 1171–1177 (1993)
56. Braeuning, S., Jelmert, T.A., Vik, S.A.: The effect of the quadratic gradient term on variable-rate well-tests. J. Pet. Sci. Eng. **21**, 203–222 (1998)
57. Li, W., Li, X.P., Li, S.C., et al.: The similar structure of solutions in fractal multilayer reservoir including a quadratic gradient term. J. Hydrodyn. **24**, 332–338 (2012)
58. Dewei, M., Ailin, J., Chengye, J., et al.: Research on transient flow regulation with the effect of quadratic pressure gradient. Pet. Sci. Technol. **31**, 408–417 (2013)
59. Nie, R.S., Ge, F., Liu, Y.L.: The researches on the nonlinear flow model with quadratic pressure gradient and its application for double porosity reservoir. In: Flow in porous media: from phenomena to engineering and beyond: 2009 International Forum on Porous Flow and Applications. Wuhan (2009)
60. Yao, Y.D., Wu, Y.S., Zhang, R.L.: The transient flow analysis of fluid in a fractal, double-porosity reservoir. Transp. Porous Media **94**, 175–187 (2012)
61. Nie, R.S., Jia, Y.L., Yu, J., et al.: The transient well test analysis of fractured-vuggy triple-porosity reservoir with the quadratic pressure gradient term. In: Latin American and Caribbean Petroleum Engineering Conference. Cartagena de Indias (2009)
62. Crank, J.: Free and Moving Boundary Problems. Clarendon Press, Oxford (1984)
63. Gupta, R.S., Kumar, A.: Treatment of multi-dimensional moving boundary problems by coordinate transformation. Int. J. Heat Mass Transf. **28**, 1355–1366 (1985)
64. Méndez-Bermúdez, A., Luna-Acosta, G.A., Izrailev, F.M., et al.: Solution of the eigenvalue problem for two-dimensional modulated billiards using a coordinate transformation. Commun. Nonlinear Sci. Numer. Simul. **10**, 787–795 (2005)
65. Burden, R.L., Faires, J.D.: Numerical Analysis, 9th edn. Brooks/Cole, West Lafayette (2010)
66. Poularikas, A.D.: The Handbook of Formulas and Table for Signal 'Processing, the Electrical Engineering Handbook Series. CRC Press LLC and IEEE Press, New York (1999)
67. McCollum, P.A., Brown, B.F.: Laplace Transform Tables and Theorems. Holt Rinehart and Winston, New York (1965)
68. Podlubny, I.: Fractional Differential Equations. Academic Press, San Diego (1999)